Chapter 1

Comparison of chaotic biomagnetic field patterns recorded from the arrhythmic heart and stomach

Andrei Irimia, Michael R. Gallucci, John P. Wikswo Jr.
Living State Physics Laboratories, Vanderbilt University
andrei.irimia@vanderbilt.edu

We here investigate the time evolution of normal and arrythmic cardiac and gastric biomagnetic signals using simultaneous magnetocardiography (MCG) and magnetogastrography (MGG). Noninvasive MCG/MGG recordings were acquired from ten anesthetized domestic pigs in the control (healthy) state. Thereafter, gastric arrhythmia was induced via surgical stomach division, which disrupted the natural periodicity of the gastric musculature activation cycle. After recording biomagnetic data in this state for one hour, cardiac arrythmia was induced in each anesthetized pig, which allowed us to compare cardiac and gastric arrhythmia within the framework of an intra-subject animal model. Signal analysis revealed that several features are shared by cardiac and gastric arrhythmias, particularly with respect to the chaos content of the magnetic signal from each organ before and after the onset of pathophysiology. Our findings indicate that chaos phenomena in the gut−which have been investigated only recently−may be similar to those in the heart, which are better understood. [1]

[1]Funding was provided by NIH grants R01 DK 58697 and 58197 and by the New England Complex Systems Institute.

1.1 Introduction

In recent years, much progress has been made in the direction of turning chaos theory into a reliable tool for the characterization of cardiac pathophysiology, particularly in the context of fibrillation and heart failure [2, 5]. Investigations of magnetically-recorded chaotic patterns from the mammalian heart and gut are important for the elucidation of complex pathological states such as arrhythmia, ischemia and muscle injury. Whereas cardiac physiology has been studied extensively using nonlinear analysis methods, little has been done to investigate the nature of such conditions in the gastrointestinal (GI) system, where their clinical significance is nevertheless comparable. In the normal heart, the sinus node acts as a pacemaker and abnormal rhythmicity in the node can lead to cardiac arrythmia. In the case of the stomach, gastric electrical activity (GEA) possesses a pacemaker as well, which is located in the gastic antrum. There, the interstitial cells of Cajal impose periodic waves of cell membrane depolarization and repolarization that advance along the corpus of the stomach at a rate of 3-6 cycles per minute (cpm) in porcines. Each of these waves consists of a potential upstroke followed by a plateau and then by a sustained depolarization phase. In this study, we compare the time evolution of normal and arrythmic cardiac and gastric biomagnetic signals using simultaneous magnetocardiography (MCG) and magnetogastrography (MGG) and discuss the similarities and differences between the two. Moreover, we quantify normality and pathology in the two organs using various measures, both visual (Lorentz attractors, 2D return maps) and quantitative (capacity dimension, correlation integral, etc). Finally, we report statistically significant differences in these quantitative measures between the normal and pathological states.

1.2 Experimental protocol

Our study made use of two noninvasive techniques called magnetocardiography (MCG) and magnetogastrography (MGG). The use of MGG is arguably more advantageous than that of electrogastrography (EGG) because the quality and strength of recorded EGG signals are strongly dependent upon the permittivity of tissues, whereas MGG depends primarily on their permeability, which is approximately equal to that of free space. EGG signals are thus attenuated by the layers of fat and skin located between internal organs and the recording electrodes, while MGG does not suffer from this setback [6].

Because gastric biomagnetic fields are very weak ($\mathcal{O}(10^{-12})$ T), signals were acquired using a Superconducting QUantum Interference Device (SQUID) biomagnetometer. The multichannel 637i SQUID biomagnetometer (Tristan Technologies Inc., San Diego, CA, USA) in the Vanderbilt University Gastrointestinal SQUID Technology (VU-GIST) Laboratory has detection coils located at the bottom of a dewar filled with liquid helium. The coils are magnetically coupled to the SQUID coils, which convert magnetic flux incident on the detection coils to voltage signals that are amplified and then acquired at 3 kHz. The detection

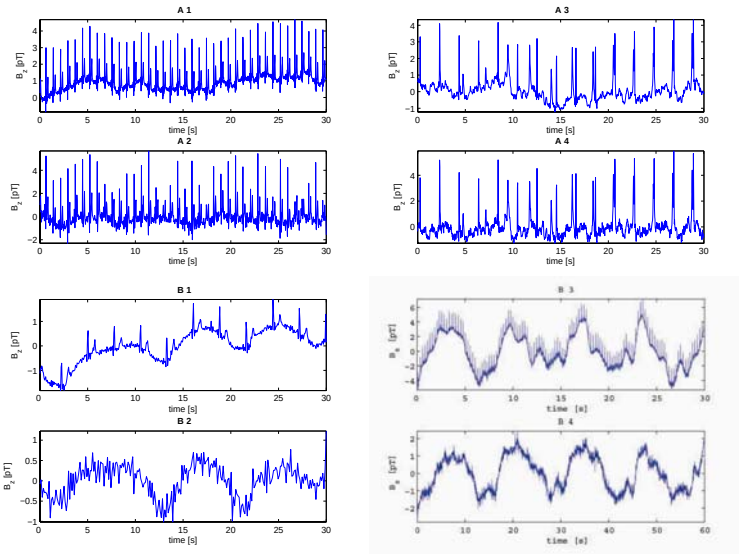

Figure 1.1: Sample normal and pathological magnetic signals for the heart (A1-A4) and stomach (B1-B4) acquired from a porcine subject. The first column contains normal signals while the second one displays pathological signals. A1 and B1 show *normal* raw magnetic field (B_z) data, while A2 and B2 show FICA-processed, artifact-reduced signals. Similarly, A3 and B3 display *pathological* raw magnetic field (B_z) signals, while A4 and B4 show FICA-processed, artifact-reduced pathological data.

coils are arranged in gradiometer format as a horizontal grid. Each anesthetized animal subject was placed horizontally under the SQUID inside a magnetically shielded room. Our protocol was approved by the Vanderbilt University Institutional Animal Care and Use Committee (VU-IACUC). The animal subject set consisted of 10 healthy domestic pigs (*sus domesticus*) of approximately 20 kg each. Initial anaesthesia consisted of intravenous injections of Telazol, Ketamine and Xylazine, each at a concentration of 100 mg/ml. The dosage administered was 4.4 mg/kg Telazol, 2.2 mg/kg Ketamine and 2.2 mg/kg Xylazine. Each animal was intubated and maintained on isoflurane anaesthesia with a concentration of 1.5-2.5%. Because the extent of the SQUID input grid is comparable to the size of the animal's chest and abdomen, simultaneous MCG/MGG signals could be recorded. In each pig, the stomach was surgically divided (which led to gastric electrical source uncoupling) and post-division data were acquired. After one hour of post-surgery recording time, cardiac arrythmia was induced in pigs using an intravenous injection as data were being acquired. All animals were under monitored anaesthesia while this was done. The injected solution consisted of pentobarbital sodium with a concentration of 390 mg/ml and a dosage of 86 mg/kg (1 cc/10 lb). This procedure allowed us to record not only the abnormal gastric signals of each pig resulting from stomach division, but also the arrhythmic cardiac signals induced by the injection. The signals from the

two organs were recorded simultaneously.

1.3 Analysis methods

Both visual (attractors, Poincaré return maps, etc.) and numerical (capacity and correlation dimensions, etc.) tools were employed to quantify the time evolution of chaos patterns during arrhythmia. First, we made use of fast independent component analysis (fast ICA) to recover the cardiac and gastric sources of interest from the SQUID-recorded mixtures. In [4] we demonstrated the use of ICA for noninvasive MGG signal processing. The dimensionality of each data set was first reduced using principal component analysis (PCA), whereafter fast ICA was applied. PCA is a technique that describes the variation of a multivariate data set in terms of a set of uncorrelated variables, each of which is a particular linear combination of the original variables [1]. The principal components (PCs) of PCA are linear combinations of the underlying variables in the data set that maximize the variance of each PC subject to an orthonormality constraint. We used the fast ICA algorithm of Hyvärinen and Oja [3], which minimizes the mutual information between the random variables that define the separated signals of interest. A detailed description of our approach to implement FastICA is available in [4].

Lorentz attractors were used to visualize our MCG/MGG data. These three-dimensional objects can be formally defined as the subspace of the total state space of a system to which the trajectory of the system converges after the initial transients have died out [7]. Differences in attractor characteristics between the healthy and pathological states were quantified numerically using four measures, namely the capacity dimension, information dimension, correlation dimension and correlation integral. A 3D attractor can be divided using a partition of boxes of edge length ϵ. If $N(\epsilon)$ is the minimum number of boxes required to cover the spatial extent of the attractor, the capacity dimension of the system can be defined as

$$C = \lim_{\epsilon \to 0} \frac{\ln N(\epsilon)}{\ln(1/\epsilon)}. \tag{1.1}$$

The second measure that was used is the Balatoni-Rényi information dimension δ, which is a generalization of the capacity dimension concept that weighs each non-empty cube i by its probability p_i:

$$\delta = \lim_{\epsilon \to 0} \frac{1}{\ln \epsilon} \sum_{i=1}^{N(\epsilon)} p_i \ln(1/p_i). \tag{1.2}$$

Another popular measure is the correlation dimension

$$\nu = \lim_{\epsilon \to 0} \frac{\ln \mathcal{I}}{\ln \epsilon}, \tag{1.3}$$

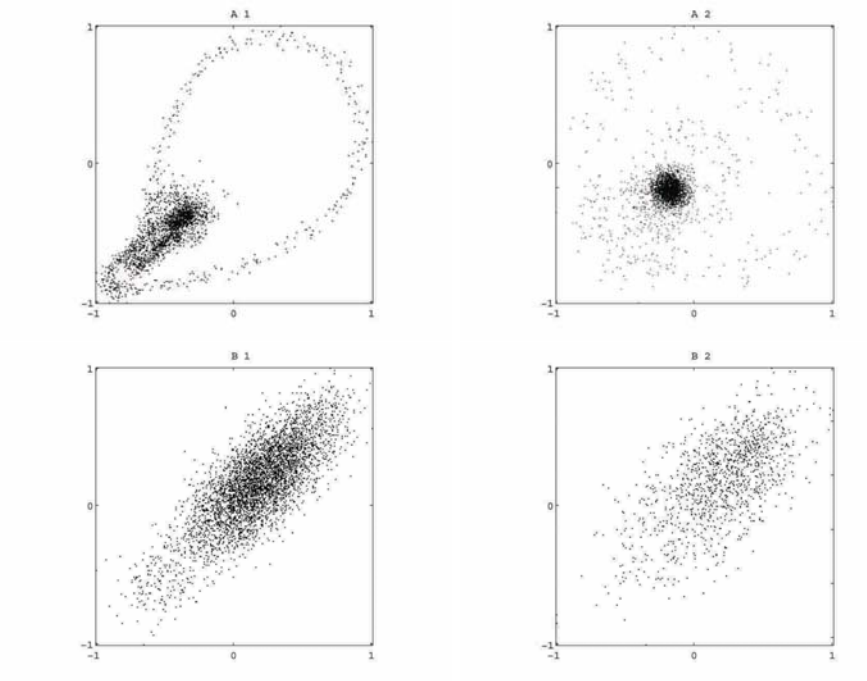

Figure 1.2: Sample return maps for SQUID signals recorded from the heart (A) and stomach (B) of a domestic pig. The first column contains maps created from normal data while the second one displays maps from pathological data. Each signal $s(t)$ was normalized for simplicity with respect to $\max\{s(t)\}$ before generating the map.

where $\mathcal{I}(\epsilon)$ is the correlation integral

$$\mathcal{I}(\epsilon) = \lim_{N\to\infty} \frac{1}{N(N-1)} \sum_{i=1}^{N} \sum_{j=1}^{N} \Theta(\epsilon - |\mathbf{r}_i - \mathbf{r}_j|), \tag{1.4}$$

Above, $\Theta(x)$ is the Heaviside function (-1 if $x \geq 0$, 0 otherwise) and $|\mathbf{r}_i - \mathbf{r}_j|$ is the distance between two points $\mathbf{r}_i$ and $\mathbf{r}_j$.

1.4 Results and discussion

Sample raw and ICA-processed MCG and MGG signals acquired from a porcine subject are shown in Figure 1. What can be concluded from the analysis of this figure is that the underlying properties of the two biological sources are more readily apparent from their respective ICs (A2, A4, B2, B4) than from the raw data traces (A1, A3, B1, B3). Although cardiac interference (A1) is a significant artifact in the gastric signals of (B1), its presence was reduced via FICA. In A3 and A4, arrhythmic heart signals are shown while B3 and

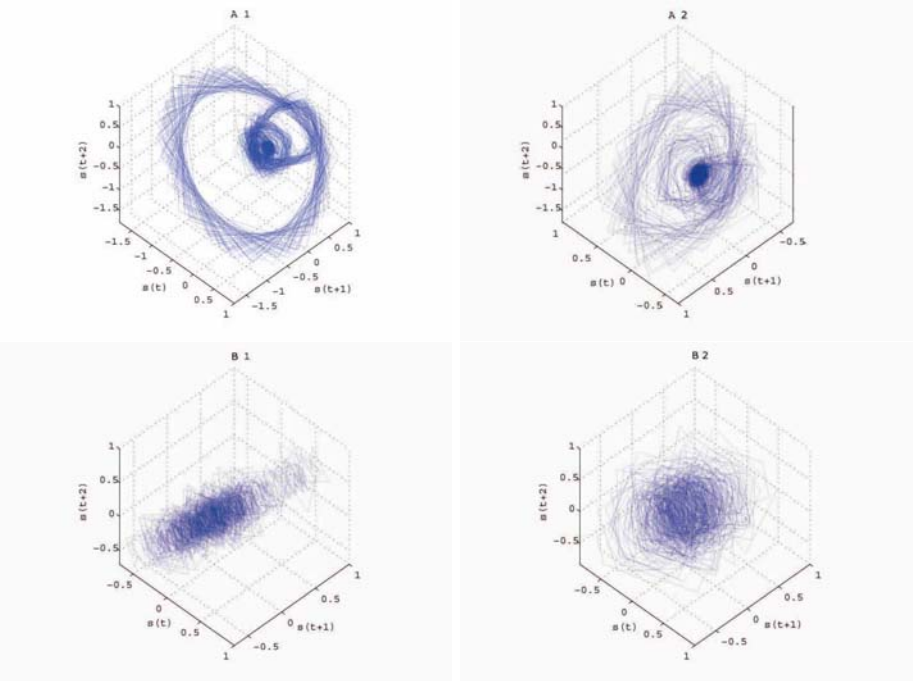

Figure 1.3: Example of Lorenz attractors for heart (A) and stomach (B) signals. Both normal (1) and pathological (2) data were used and normalization was applied as in the previous figure.

B4 display a tachygastric signal induced by stomach division. The differences between the normal and pathological signals of the heart are readily visible from our figure. Whereas the periodicity of the PQRST complex in the first case is normal ((A1) and (A2)), pronounced bradycardia is visible in (A3) and (A4). In the case of the gastric signals, the dominant GEA frequency is of approximately 3 cpm in (B1) and (B2), whereas (B3) and (B4) show a tachygastric rhythm of approximately 4.5 cpm.

Sample Poincaré return maps are displayed in Figure 3 and examples of Lorentz attractors created from our data are shown in Figure 4. The normal cardiac attractor (A1) has a characteristic shape due to the high rhythmic pattern of the heart signal. This feature is disrupted in the arrhythmic state, which is also reflected in the attractor (A2), which has a more irregular shape. Comparing normal (B1) and abnormal (B2) gastric signals, one can see that a larger amount of chaos is present in the abnormal case (B2) compared to (B1).

To ascertain the reliability of our quantitative measures, we analyzed their convergence as a function of ϵ. The results of this analysis for one case are shown in Figure 5. There, the definition used for the percentage error between two successive (previous vs. current) values of each measure was (current - previous) $\times$ 100 / max {previous, current}. Values on the abscissa are shown in units of

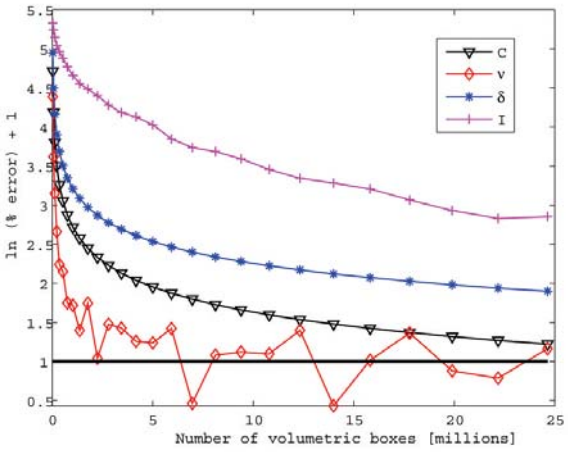

Figure 1.4: Convergence of the capacity dimension C, information dimension δ, correlation dimension ν and correlation integral $\mathcal{I}$ as a function of the number of volumetric boxes used for their computation (see text for details). The definition used for the percentage error between two successive (previous vs. current) values of each measure was (current - previous) $\times$ 100 / max {previous, current}. Values on the abscissa are shown in units of ln (% error) + 1, such that no error (perfect agreement) corresponds to the horizontal line $y = 1$, which is also drawn.

ln (% error) + 1, such that perfect agreement corresponds to the horizontal line $y = 1$. As the figure shows, all four measures were found to converge, albeit at different rates. The convergence of ν was found to be rapid, although oscillatory behavior was found to exist when more than 5×10^6 boxes were used for its computation. On the other hand, both C and δ were found to converge smoothly for this example, although much slower than ν. The correlation integral $\mathcal{I}$, which is the most computationally-intensive measure, was found in general to have a predictable behavior.

For most of our data samples, δ was found to best reflect the differences between the healthy and pathological states. Because of this, we focus on the behavior of this parameter throughout the remainder of our discussion. In the case of MGG recordings from normal subjects, because GEA parameters such as frequency and amplitude are approximately constant in time, δ was found to be well behaved, with a normalized variance ($\sigma(\delta)/\langle\delta\rangle$) of 0.12 $\langle\delta\rangle$ across subjects. In the case of pathology, arrhythmia was found to cause abrupt and frequent changes in GEA parameters, which was reflected in the normalized variance of δ having a value of 0.84 $\langle\delta\rangle$ across subjects. These differences in δ were found to be statistically significant ($p < 0.001$). Normalized variances are reported here instead of absolute numbers because the σ statistic was computed across subjects, where large inter-subject differences in δ were found although the time behavior of this parameter was found to be very similar in all cases.

1.5 Conclusion

In conclusion, we have compared cardiac and gastric biomagnetic signals as recorded by simultaneous magnetocardiography and magnetogastrography. It was found that statistically significant differences in the variances of the parameter δ exist between the healthy and pathological states of the stomach and that these differences are also reflected by the visualization modalities that were presented. In the case of visual measures, distinguishable differences in attractor shape were found between the healthy and pathological states. It is our hope that further study of such differences may one day help us develop novel methods for the noninvasive characterization of gastric disease.

1.6 Acknowledgments

Research funding was provided by NIH grants R01 DK58697 and DK58197 (AI and MRG) and HL58241 (JPW). We are grateful to the Graduate School of Arts and Sciences at Vanderbilt University and to the New England Complex Systems Institute for covering travel expenses to Boston for the first author. Cheryl Cosby and Allison Price provided essential administrative support. We also wish to thank Phil Williams and Amy Grant from the Surgical Research Division at the Vanderbilt University Medical Center for their assistance with our animal experiments. Richard A Gray from the Department of Biomedical Engineering at the University of Alabama at Birmingham provided insightful suggestions regarding the content of the article.

Bibliography

[1] BS Everitt and G Dunn (1992) Applied multivariate data analysis *Oxford University Press* New York, NY 45-64

[2] AL Goldberger, LAN Amaral, JM Hausdorff, PC Ivanov, CK Peng, HE Stanley (2002) Fractal dynamics in physiology: alterations with disease and aging *Proc Natl Acad Sci USA* vol 99 2466-2472

[3] A Hyvärinen and E Oja (1997) A fast fixed-point algorithm for independent component analysis *Neural Comput* vol 9 1483-1492

[4] A Irimia, LA Bradshaw (2005) Artifact reduction in magnetogastrography using fast independent component analysis *Physiol Meas* vol 26 1059-1073

[5] PC Ivanov, LAN Amaral, AL Goldberger, S Havlin, MG Rosenblum, ZR Struzik, HE Stanley (1999) Multifractality in human heartbeat dynamics *Nature* vol 399 461-465

[6] MP Mintchev, A Stickel, KL Bowes (1998) Dynamics of the level of randomness in gastric electrical activity *Digest Dis Sci* vol 43 953-956

[7] CJ Stam (2005) Nonlinear dynamical analysis of EEG and MEG: review of an emerging field *Clin Neurophysiol* vol 116 2266-2301